J. Fluid Mech. (1984), *vol.* 148, *pp.* 225–246
Printed in Great Britain

Turbulent airflow over water waves – a numerical study

By M. A. AL-ZANAIDI† AND W. H. HUI
Department of Applied Mathematics, University of Waterloo, Ontario, Canada

(Received 27 September 1983 and in revised form 7 June 1984)

Turbulent airflow over a Stokes water-wave train of small amplitude is studied numerically based on the two-equation closure model of Saffman & Wilcox (1974) together with appropriate boundary conditions on the wave surface. The model calculates, instead of assuming, the viscous sublayer flow, and it is found that the energy transfer between wind and waves depends significantly on the flow being hydraulically rough, transitional or smooth. Systematic computations have yielded a simple approximate formula for the fractional rate of growth per radian

$$\zeta = \delta_i \frac{\rho}{\rho_w}\left(\frac{U_\lambda}{c}-1\right)^2,$$

with $\delta_i = 0.04$ for transitional or smooth flow and $\delta_i = 0.06$ for rough flow, where ρ is density of air, ρ_w that of water, U_λ wind speed at one wavelength height and c the wave phase velocity. This formula is in good agreement with most existing data from field experiments and from wave-tank experiments. In the case of waves travelling against wind, the corresponding values are $\delta_i = -0.024$ for transitional and smooth flow, and $\delta_i = -0.04$ for rough flow.

1. Introduction

The question of how wind blowing over the surface of water generates waves remains a central problem in wind–wave research, despite the large amount of theoretical and experimental work during the last decades.

Ingenious methods have been devised to measure the growth rates due to the direct input of energy from wind to waves in wave tanks by Shemdin & Hsu (1967), Larson & Wright (1975), Wu, Hsu & Street (1977, 1979) and Kawai (1979), and on the ocean by Dobson (1971), Elliott (1972), Snyder (1974), and Snyder *et al.* (1981). These results, despite large scattering, have been shown recently by Plant (1982) to be well described by a simple empirical formula for the fractional rate of energy input by wind per radian ζ:

$$\zeta \equiv \frac{\beta}{\sigma} = (0.04 \pm 0.02)\left(\frac{u_*}{c}\right)^2, \tag{1}$$

where u_* is the friction velocity of the wind, σ and c are the frequency and phase velocity of the waves travelling in the same direction as the wind, and β is defined in (40*a*).

On the theoretical side, whilst Phillips' (1957) resonant theory of wave generation by wind describes the initial stage of generation when the wave amplitude is extremely small and the growth is linear in time, it is well documented that, in the

† Present address: Department of Mathematics, University of Kuwait.

more important stage of generation, the wave grows exponentially in time. Miles' (1957, 1959) inviscid theory does predict an exponential growth, but it tends to underestimate the growth rate by a factor of 2 to 3 when compared with measurements. It is well recognized that in Miles' inviscid theory the air-flow turbulence, which is necessarily present in the field, is largely neglected, except in its role in setting up the logarithmic shear flow. This neglect of turbulent effects in the theory has been ascribed (Miles 1967) to be the main reason for the large differences between theory and experiments, and attempts were made by Davis (1969, 1970, 1972, 1974) among others to extend Miles' theory to include these effects numerically. It was found that the energy-transfer rate so calculated depended sensitively on the closure model employed and on the details of the velocity profile assumed in the viscous sublayer near the surface. Riley, Donelan & Hui's (1982) extension of Miles' theory to include the effect of interaction of waves with turbulence based on Prandtl's mixing-length hypothesis improves the growth rate only slightly.

Numerical calculations of the rate of energy input from the turbulent airflow to water waves were made by Townsend (1972), Gent & Taylor (1976) and Gent (1977). These studies assumed a rough flow and used a one-equation closure model. Whilst the rough-flow assumption is quite valid in many wave-tank experiments, it is also known that turbulent airflow over water waves on the ocean (Snyder *et al.* 1981) and in some laboratory situations (Hsu *et al.* 1982) is typically transitional and not rough. On the closure model, experience (Launder & Spalding 1972) has shown that one-equation closure models are only marginally more accurate than Prandtl's mixing-length hypotheses, and that two-equation closure models are more accurate. Furthermore, a recent survey by Marvin (1983) concluded that modelling through eddy-viscosity concepts will probably be sufficient for most two-dimensional attached flow over solid boundaries. It was therefore decided to use a two-equation closure model to compute the turbulent flow over a Stokes wavetrain of small amplitude for which the airflow over the waves is attached.

There are several versions of the two-equation closure model (for a survey see e.g. Marvin 1983; Launder & Spalding 1972), which are all similar in that they all assume the turbulence to be characterized by two densities which obey two diffusion equations. They otherwise all differ in details. The version of the two-equation closure model due to Saffman & Wilcox (1974) is chosen here mainly because it is also capable of calculating the viscous-sublayer flow near the wave surface, in addition to its being well tested against experiments of flow over solid surfaces in many known cases.

The governing equations and boundary conditions based on this model, and the numerical method for solving them are described in §2. It turned out (§3) that the growth rate under rough flow conditions is typically 50% higher than that under transitional flow conditions. Systematic calculations also lead to a simple formula (49) for the growth rate which is in good agreement with experiments.

2. Mathematical formulation

2.1. *The model equations of Saffman & Wilcox*

Consider an incompressible, statistically steady and fully developed turbulent airflow over deep-water gravity waves. Let the system of Cartesian coordinates (x_1, x_2) be such that the x_2 axis is directed vertically upwards and measures from the mean water surface. The waves are periodic in x_1, with wavelength λ and of Stokes type, and propagate along the x_1 direction with uniform effective surface roughness length y_0.

As is standard, the velocity $\boldsymbol{V}$ (the local Eulerian velocity) is separated into a mean velocity $\boldsymbol{U}$ and a fluctuating part $\boldsymbol{u}$ as $V_i = U_i + u_i$ $(i = 1, 2)$. The pressure is separated similarly as $p = \bar{P} + p'$. Substitution of these expressions into the continuity and momentum equations and averaging with respect to time (denoted by an overbar) give the required equations for the mean turbulent flow. In a frame of reference moving with the wave phase velocity c, the mean flow is steady and the governing equations are

continuity equation

$$\frac{\partial U_i}{\partial x_i} = 0; \tag{2}$$

momentum equations

$$U_j \frac{\partial U_i}{\partial x_j} = -\frac{\partial P}{\partial x_i} + \frac{\partial}{\partial x_j}[2(\nu + \epsilon) S_{ij}], \quad i, j = 1, 2, \tag{3}$$

where $P = (1/\rho)\bar{P} + \frac{2}{3}E$. In (3) ρ and ν are the density and kinematic viscosity of the air respectively, and

$$E = \tfrac{1}{2}\overline{u_i u_i} \tag{4}$$

is the specific turbulent kinetic energy.

In (3) the assumption of an eddy viscosity is used whereby the mean transfer of momentum by Reynolds stress is described by a scalar eddy viscosity ϵ; that is, the Reynolds-stress tensor is

$$-\rho\,\overline{u_i u_j} = 2\rho\epsilon S_{ij} - \tfrac{2}{3}\rho E \delta_{ij}, \tag{5}$$

where

$$S_{ij} = \frac{1}{2}\left[\frac{\partial U_i}{\partial x_j} + \frac{\partial U_j}{\partial x_i}\right] \tag{6}$$

is the rate-of-strain tensor and δ_{ij} the Kronecker delta. Equation (5) represents the first hypothesis made in the model of Saffman & Wilcox (1974) as it is in any other two-equation closure model. The theoretical justification of the assumption of eddy viscosity is that the eddy-viscosity hypothesis is equivalent to retaining the leading term in an expansion of the (unknown) functional relation between Reynolds stresses and the mean-velocity distribution (Saffman 1970). As noted earlier, the sufficiency of the eddy-viscosity model was well demonstrated by Marvin (1983) for attached two-dimensional flow over solid boundaries.

The second common hypothesis made in the two-equation closure models is that the components of the turbulence responsible for the mixing and transfer of momentum are determined by an energy density E and pseudovorticity density ω, which satisfy nonlinear diffusion equations. In the version of Saffman & Wilcox these are

turbulent-energy equation

$$U_j \frac{\partial E}{\partial x_j} = E[b_1 (2 S_{ij} S_{ij})^{\frac{1}{2}} - b_2 \omega] + \frac{\partial}{\partial x_j}\left[(\nu + b_3 \epsilon)\frac{\partial E}{\partial x_j}\right]; \tag{7}$$

turbulent-pseudovorticity equation

$$U_j \frac{\partial \omega^2}{\partial x_j} = \omega^2\left[b_4 \left(\frac{\partial U_i}{\partial x_j}\frac{\partial U_i}{\partial x_j}\right)^{\frac{1}{2}} - b_5 \omega\right] + \frac{\partial}{\partial x_j}\left[(\nu + b_6 \epsilon)\frac{\partial \omega^2}{\partial x_j}\right]; \tag{8}$$

where $b_1, b_2, \ldots, b_6$ are constants. The values of these six constants in the transport

equations are fixed with general arguments by Saffman (1970) and Saffman & Wilcox (1974). They are

$$\left.\begin{aligned} b_3 = b_6 = 0.5, \quad b_1 = 0.3, \quad b_2 = b_1^2, \\ \frac{5}{3} < \frac{b_5}{b_2} < 2, \\ b_4 = b_1\left(\frac{b_5}{b_2} - \frac{4b_6}{b_1}\kappa^2\right), \end{aligned}\right\} \tag{9}$$

where κ ($= 0.41$) is the von Kármán constant and $b_5 = 1.8b_2$ is used in this paper.

This set of constants have been shown by Saffman & Wilcox to yield accurate calculation for the entire boundary-layer flow over a flat plate, including the prediction of the von Kármán constant in the law of the wall.

The system of equations (2), (3), (7) and (8) is closed by the relation

$$\epsilon = E/\omega, \tag{10}$$

which is obtained from dimensional consideration of the local properties of the turbulence being determined by the energy density E and the pseudovorticity ω.

As shown by Saffman (1970), the transport equations (7) and (8), which are similar to the set proposed by Kolmogorov (1942), incorporate the essential physical ideas that turbulence is convected by the mean flow, amplified by interaction with a mean-velocity gradient, diffused owing to the interaction of the turbulence with itself, and dissipated also owing to self-interaction. The model equations have been extended by Saffman & Wilcox (1974) to compressible turbulent flow, yielding the Van Driest compressible law of the wall.

2.2. *Transformation to curvilinear coordinates*

We now use a system of orthogonal curvilinear coordinates (ξ, η) that is moving with the wave, in which the wave surface is a coordinate line $\eta = 0$, to overcome the difficulties arising from applying the surface boundary conditions. Therefore let

$$\left.\begin{aligned} x_1 &= \xi - \mathrm{Re}\,[ia\exp\{ik(\xi + i\eta)\}], \\ x_2 &= \eta - \mathrm{Re}\,[a\exp\{ik(\xi + i\eta)\}], \end{aligned}\right\} \tag{11}$$

where a and k ($= 2\pi/\lambda$) are respectively the amplitude and the wavenumber of the wave. To second order in the wave slope ak, the coordinate $\eta = 0$ corresponds to the shape of the Stokes wave in deep water, that is

$$x_2 = -a\cos kx_1 - \tfrac{1}{2}a^2k\sin^2 kx_1 + O(a^3k^2). \tag{12}$$

The Jacobian of the transformation is

$$J = \frac{\partial(\xi, \eta)}{\partial(x_1, x_2)} = [1 + 2ak\,\mathrm{e}^{-k\eta}\cos k\xi + (ak)^2\,\mathrm{e}^{-2k\eta}]^{-1}. \tag{13}$$

In what follows, all the velocities are scaled by the friction velocity u_* and lengths by ν/u_*. The governing equations in §2.1 when transformed to (ξ, η)-variables become as follows:

continuity equation

$$\frac{\partial}{\partial\xi}(J^{-\frac{1}{2}}u) + \frac{\partial}{\partial\eta}(J^{-\frac{1}{2}}v) = 0, \tag{14}$$

where u and v are the mean velocities in the ξ- and η-directions;

momentum equations

$$\frac{\partial}{\partial\xi}(J^{-1}uu)+\frac{\partial}{\partial\eta}(J^{-1}uv)+\tfrac{1}{2}J^{-2}(u^2+v^2)\frac{\partial J}{\partial\xi}+J^{-1}\frac{\partial P}{\partial\xi}$$
$$=\frac{\partial}{\partial\xi}\left[J^{-1}\left(1+\frac{E}{\omega}\right)\left\{\frac{\partial}{\partial\xi}(J^{\frac{1}{2}}u)-\frac{\partial}{\partial\eta}(J^{\frac{1}{2}}v)\right\}\right]+\frac{\partial}{\partial\eta}\left[J^{-1}\left(1+\frac{E}{\omega}\right)\left\{\frac{\partial}{\partial\eta}(J^{\frac{1}{2}}u)+\frac{\partial}{\partial\xi}(J^{\frac{1}{2}}v)\right\}\right], \tag{15}$$

$$\frac{\partial}{\partial\xi}(J^{-1}uv)+\frac{\partial}{\partial\eta}(J^{-1}vv)+\tfrac{1}{2}J^{-2}(u^2+v^2)\frac{\partial J}{\partial\eta}+J^{-1}\frac{\partial P}{\partial\eta}$$
$$=\frac{\partial}{\partial\xi}\left[J^{-1}\left(1+\frac{E}{\omega}\right)\left\{\frac{\partial}{\partial\eta}(J^{\frac{1}{2}}u)+\frac{\partial}{\partial\xi}(J^{\frac{1}{2}}v)\right\}\right]-\frac{\partial}{\partial\eta}\left[J^{-1}\left(1+\frac{E}{\omega}\right)\left\{\frac{\partial}{\partial\xi}(J^{\frac{1}{2}}u)-\frac{\partial}{\partial\eta}(J^{\frac{1}{2}}v)\right\}\right]; \tag{16}$$

energy equation

$$J^{-\frac{1}{2}}u\frac{\partial E}{\partial\xi}+J^{-\frac{1}{2}}v\frac{\partial E}{\partial\eta}$$
$$=J^{-1}E[b_1(R_t^2+R_n^2)^{\frac{1}{2}}-b_2\omega]+\frac{\partial}{\partial\xi}\left[\left(1+\frac{b_3E}{\omega}\right)\frac{\partial E}{\partial\xi}\right]+\frac{\partial}{\partial\eta}\left[\left(1+\frac{b_3E}{\omega}\right)\frac{\partial E}{\partial\eta}\right]; \tag{17}$$

pseudovorticity equation

$$J^{-\frac{1}{2}}u\frac{\partial\omega^2}{\partial\xi}+J^{-\frac{1}{2}}v\frac{\partial\omega^2}{\partial\eta}$$
$$=J^{-1}\omega^2(b_4S_\omega^{\frac{1}{2}}-b_5\omega)+\frac{\partial}{\partial\xi}\left[\left(1+\frac{b_6E}{\omega}\right)\frac{\partial\omega^2}{\partial\xi}\right]+\frac{\partial}{\partial\eta}\left[\left(1+\frac{b_6E}{\omega}\right)\frac{\partial\omega^2}{\partial\eta}\right]; \tag{18}$$

where
$$\left.\begin{aligned}R_t&=\frac{\partial}{\partial\eta}(J^{\frac{1}{2}}u)+\frac{\partial}{\partial\xi}(J^{\frac{1}{2}}v),\quad R_n=\frac{\partial}{\partial\xi}(J^{\frac{1}{2}}u)-\frac{\partial}{\partial\eta}(J^{\frac{1}{2}}v),\\ S_\omega&=\tfrac{1}{2}(R_t^2+R_n^2)+\tfrac{1}{2}J^2\left[\frac{\partial}{\partial\eta}(J^{-\frac{1}{2}}u)-\frac{\partial}{\partial\xi}(J^{-\frac{1}{2}}v)\right]^2.\end{aligned}\right\} \tag{19}$$

2.3. *Boundary conditions*

The boundary conditions of turbulent airflow over the water wave moving with phase velocity c can be divided into two groups: those on the surface of the wave and those far away from the wave surface. The outer conditions express the requirement that the flow disturbance due to the presence of the wave dies out for large values of the non-dimensional height. They are

$$\left.\begin{aligned}&u=\frac{1}{\kappa}\ln(1+\eta)+B,\quad v=0,\\ &P=0,\quad E=\frac{1}{b_1},\quad \omega=\frac{1}{\kappa b_1\eta}\end{aligned}\right\}\quad\text{as } \eta\to\infty, \tag{20}$$

where B is the constant in the law of the wall, whose value depends upon the roughness of the surface. Experimental results have well confirmed the validity of the logarithmic distribution of mean wind velocity away from the wave.

The second group of the boundary conditions are the inner conditions (on the wave surface). As mentioned before, Davis (1972) showed how sensitively the energy

transfer between wind and wave is dependent on the assumed form of wind velocity in the sublayer. It should be pointed out that the wind velocity in the sublayer must be determined from the interactions of airflow and wave motion and cannot be assumed *a priori*. Moreover, the effect of the viscous sublayer was shown by Stewart (1970) to be important near the water surface. It is thus essential to impose correct boundary conditions at the wave surface in order to calculate the viscous sublayer. The boundary conditions that will be imposed on the wave surface are

$$u = -cJ^{-\frac{1}{2}}, \quad v = 0, \quad E = 0 \quad (\eta = 0), \tag{21a,b,c}$$

and a boundary condition on ω to be discussed later. Equation (21*a*) expresses that the mean tangential velocity equals the velocity of the wave plus the orbital velocity of the water particle.†

The condition for the pseudovorticity at a solid surface was proposed by Saffman & Wilcox (1974) in terms of a universal function of roughness for the case of a flat plate

$$\omega = \frac{Q(u_* y_0/\nu)}{b_1} \quad (\eta = 0), \tag{22}$$

where y_0 is the roughness length and $Q(u_* y_0/\nu)$ is a universal function of the roughness parameter $u_* y_0/\nu$. The surface pseudovorticity condition (22) of Saffman & Wilcox (1974) for a flat surface needs to be modified to include the effect of a wavy surface. The presence of the wave must cause variation of ω along the surface. To find this variation, we take the pseudovorticity to behave like vorticity (i.e. $\boldsymbol{\omega} \sim \operatorname{curl} \boldsymbol{V}$). Since the vorticity $\operatorname{curl} \boldsymbol{V}$ changes under the transformation to the orthogonal coordinates (ξ, η) by a factor J^{-1}, it is thus proposed that the boundary condition (22) be modified to

$$\omega = \frac{Q(u_* y_0/\nu) J^{-1}}{b_1} \quad (\eta = 0). \tag{23}$$

It can also be shown qualitatively that this effect of variation of ω is equivalent to the variation of surface roughness length y_0. Thus, if we write

$$y_0 = \bar{y}_0 + aky_1,$$

where $\bar{y}_0$ is the average value of y_0, and y_1 represents the first-order (in ak) correction to the roughness length y_0, then y_1 is positive at the crest and negative at the trough. Substitution of the last equation into condition (23) and using Taylor's expansion, we obtain

$$\omega = \frac{1}{b_1}\left[Q\left(\frac{u_* \bar{y}_0}{\nu}\right) + ak \frac{u_* y_1}{\nu} Q'\left(\frac{u_* \bar{y}_0}{\nu}\right)\right].$$

Since Q' is negative, as can be seen from (24), the pseudovorticity is larger at the trough and smaller at the crest. This behaviour is qualitatively the same as that of condition (23).

Three different degrees of roughness can be distinguished as follows.

(i) Hydraulically smooth ($0 \leqslant u_* y_0/\nu \leqslant 0.12$; a typical value of Q is 100). The roughness grains are entirely embedded in the sublayer.

(ii) Transitional roughness ($0.12 \leqslant u_* y_0/\nu \leqslant 2.42$; a typical value of Q is 6.3). The constant of integration B in (20) begins to decrease with the increase of $u_* y_0/\nu$.

† The Stokes drift, being of higher order, is not included in the tangential-velocity condition on the water surface. The surface wind-drift velocity, whose effects on the air flow are found by numerical experiments to be negligible (Al-Zanaidi 1982), is also ignored in (21).

(iii) Completely rough ($u_* y_0/\nu > 2.42$; a typical value of Q is 0.1). The size of the roughness elements is such that the Reynolds number of the flow in their vicinity is large, so that the viscosity of the fluid has comparatively little influence on the whole motion.

The universal function Q can be expressed in terms of the roughness parameter as follows:

$$Q\left(\frac{u_* y_0}{\beta}\right) \approx \begin{cases} 6.26\left[\ln\left(\frac{u_* y_0}{\nu}\right)+2.38\right]^{-2} & \text{(smooth and transitional)}, \\ 1.44\left[\ln\left(\frac{u_* y_0}{\nu}\right)+0.68\right]^{-2} & \text{(rough)}. \end{cases} \tag{24}$$

These relations were obtained from experimental data by Saffman & Wilcox (1974) and will be used in (23).

To sum up, the problem of calculating the turbulent airflow over a Stokes wavetrain is to solve (14)–(19) subject to boundary conditions (20), (21) and (23).

3. Linear theory and numerical calculations

3.1. *Linear theory*

We now assume that the amplitude of the Stokes wavetrain is small, so that $ak \ll 1$. With terms $O((ak)^2)$ neglected, we may write

$$\left.\begin{aligned} u(\xi,\eta) &= U_0(\eta)+ak\,U_1(\eta)\exp(\mathrm{i}K\xi), \\ v(\xi,\eta) &= ak\,V_1(\eta)\exp(\mathrm{i}K\xi), \\ P(\xi,\eta) &= ak\,P_1(\eta)\exp(\mathrm{i}K\xi), \\ E(\xi,\eta) &= E_0(\eta)+ak\,E_1(\eta)\exp(\mathrm{i}K\xi), \\ \omega(\xi,\eta) &= \omega_0(\eta)+ak\,\omega_1(\eta)\exp(\mathrm{i}K\xi), \\ J(\xi,\eta) &= 1+ak\,J_1(\eta)\exp(\mathrm{i}K\xi), \end{aligned}\right\} \tag{25}$$

where $K = \nu k/u_*$ is the non-dimensional wavenumber, and $J_1(\eta) = -2\,\mathrm{e}^{-K\eta}$, as may be obtained by expanding (13) for small ak. In (25), U_0, E_0 and ω_0 represent the turbulent airflow over the undisturbed water surface moving at uniform velocity c. The terms of order ak represent the first-order correction to the mean flow due to the presence of the water wave.

Substitution of the expansions (25) into the governing equations of motion (14)–(19) and the boundary conditions (20), (21) and (23) yield two systems of ordinary differential equations in η and their boundary conditions. The first system corresponds to turbulent air flow over an undisturbed water surface and is given by

$$\left(1+\frac{E_0}{\omega_0}\right)\frac{\mathrm{d}U_0}{\mathrm{d}\eta} = 1, \tag{26}$$

$$E_0\left[b_1\frac{\mathrm{d}U_0}{\mathrm{d}\eta}-b_2\omega_0\right]+\frac{\mathrm{d}}{\mathrm{d}\eta}\left[\left(1+\frac{b_3E}{\omega_0}\right)\frac{\mathrm{d}E_0}{\mathrm{d}\eta}\right] = 0, \tag{27}$$

$$\omega_0^2\left[b_4\frac{\mathrm{d}U_0}{\mathrm{d}\eta}-b_5\omega_0\right]+\frac{\mathrm{d}}{\mathrm{d}\eta}\left[\left(1+\frac{bE_0}{\omega_0}\right)\frac{\mathrm{d}\omega_0^2}{\mathrm{d}\eta}\right] = 0, \tag{28}$$

and the corresponding boundary conditions are

$$\left.\begin{aligned} U_0 &= \frac{1}{\kappa}\ln(1+\eta)+B-C, \\ E_0 &= \frac{1}{b_1}, \quad \omega_0 = \frac{1}{\kappa b_1 \eta} \end{aligned}\right\} \quad \text{as} \quad \eta\to\infty, \tag{29}$$

where $C = c/u^*$, and

$$E_0 = 0, \quad \omega_0 = Q\left(\frac{u_* y_0}{\nu}\right) b_1 \quad (\eta = 0). \tag{30}$$

The constant B in (29) depends on the roughness of the wave surface. The above system of equations and boundary conditions (26)–(30) form a well-posed boundary-value problem of the fifth order.

The second system of equations, obtained by equating like terms in ak, is as follows:

continuity equation

$$\frac{\partial V_1}{\partial\eta} + \mathrm{i}KU_1 = \tfrac{1}{2}\mathrm{i}KU_0 J_1; \tag{31}$$

momentum equations

$$\begin{aligned} &\frac{\partial}{\partial\eta}\left[\left(1+\frac{E_0}{\omega_0}\right)\frac{\partial U_1}{\partial\eta}\right] + \mathrm{i}K\left[\mathrm{i}K\left(1+\frac{E_0}{\omega_0}\right)-U_0\right]U_1 - \mathrm{i}KP_1 \\ &\quad + \left[\mathrm{i}K\frac{\partial}{\partial\eta}\left(1+\frac{E_0}{\omega_0}\right)-\frac{\partial U_0}{\partial\eta}\right]V_1 + \frac{\partial}{\partial\eta}\left[\frac{\partial U_0}{\partial\eta}\left(\frac{E_1}{\omega_0}-\frac{E_0\omega_1}{\omega_0^2}\right)\right] \\ &\qquad = -\tfrac{1}{2}U_0\frac{\partial}{\partial\eta}\left(1+\frac{E_0}{\omega_0}\right)\frac{\partial J_1}{\partial\eta}, \end{aligned} \tag{32}$$

$$\begin{aligned} &\frac{\partial}{\partial\eta}\left[\left(1+\frac{E_0}{\omega_0}\right)\frac{\partial V_1}{\partial\eta}\right] + \frac{\partial}{\partial\eta}\left(1+\frac{E_0}{\omega_0}\right)\frac{\partial V_1}{\partial\eta} \\ &\quad + \mathrm{i}K\left[\mathrm{i}K\left(1+\frac{E_0}{\omega_0}\right)-U_0\right]V_1 - \frac{\partial P_1}{\partial\eta} + \mathrm{i}K\frac{\partial U_0}{\partial\eta}\left(\frac{E_1}{\omega_0}-\frac{E_0\omega_1}{\omega_0^2}\right) \\ &\qquad = \tfrac{1}{2}U_0^2\frac{\partial J_1}{\partial\eta} + \mathrm{i}KJ_1\left[1+U_0\frac{\partial}{\partial\eta}\left(1+\frac{E_0}{\omega_0}\right)\right]; \end{aligned} \tag{33}$$

energy equation

$$\begin{aligned} &\frac{\partial}{\partial\eta}\left[\left(1+\frac{b_3E_0}{\omega_0}\right)\frac{\partial E_1}{\partial\eta}\right] + b_3\frac{\partial}{\partial\eta}\left[\frac{\partial E_0}{\partial\eta}\left(\frac{E_1}{\omega_0}-\frac{E_0\omega_1}{\omega_0^2}\right)\right] \\ &\quad + \left[(\mathrm{i}K)^2\left(1+\frac{b_3E_0}{\omega_0}\right)+b_1\frac{\partial U_0}{\partial\eta}-b_2\omega_0-\mathrm{i}KU_0\right]E_1 \\ &\quad + b_1E_0\frac{\partial U_1}{\partial\eta} + \left(\mathrm{i}Kb_1E_0-\frac{\partial E_0}{\partial\eta}\right)V_1 - b_2E_0\omega_1 \\ &\qquad = E_0J_1\left(\tfrac{1}{2}b_1\frac{\partial U_0}{\partial\eta}-b_2\omega_0\right)-\tfrac{1}{2}b_1U_0E_0\frac{\partial J_1}{\partial\eta}; \end{aligned} \tag{34}$$

pseudovorticity equation

$$\begin{aligned} &\frac{\partial}{\partial\eta}\left[2\omega_0\left(1+\frac{b_6E_0}{\omega_0}\right)\frac{\partial\omega_1}{\partial\eta}\right] + 2\frac{\partial}{\partial\eta}\left[(b_6E_1+\omega_1)\frac{\partial\omega_0}{\partial\eta}\right] \\ &\quad + 2\omega_0\left[(\mathrm{i}K)^2\left(1+\frac{b_6E_0}{\omega_0}\right)-\mathrm{i}KU_0+b_4\frac{\partial U_0}{\partial\eta}-\tfrac{3}{2}b_5\omega_0\right]\omega_1 + b_4\omega_0^2\frac{\partial U_1}{\partial\eta}-\frac{\partial\omega_0^2}{\partial\eta}V_1 \\ &\qquad = \omega_0^2J_1\left(\tfrac{1}{2}b_4\frac{\partial U_0}{\partial\eta}-b_5\omega_0\right). \end{aligned} \tag{35}$$

The corresponding boundary conditions are

$$\left.\begin{aligned} &U_1(\eta) = 0, \quad V_1(\eta) = 0, \\ &P_1(\eta) = 0, \quad E_1(\eta) = 0, \quad \omega_1(\eta) = 0 \end{aligned}\right\} \quad \text{as} \quad \eta \to \infty, \tag{36}$$

and

$$\left.\begin{aligned} &U_1(0) = \tfrac{1}{2}CJ_1(0), \quad V_1(0) = 0, \\ &E_1(0) = 0, \quad \omega_1(0) = -J_1(0)\,Q\left(\frac{u_* y_0}{\nu}\right) \end{aligned}\right\} \quad (\eta = 0). \tag{37}$$

These two systems are to be solved successively. The input data are the friction velocity u_*, the roughness length y_0 and the wavelength λ, or any equivalent system of three independent dimensional or non-dimensional quantities.

3.2. *Numerical methods*

The boundary-value problem (26)–(30) of turbulent airflow over an undisturbed water surface was solved numerically using a time-marching technique. Accordingly, in the numerical solution of these equations, the time derivatives are reintroduced in the energy and pseudovorticity equations. The normal distance η from the wave surface is stretched according to

$$z = \ln(1+\eta). \tag{38}$$

The new vertical distance z is then divided into N equal steps, and at each node the spatial derivatives are replaced by central-difference approximations, while a forward-difference approximation is used for the time derivatives. Equations (27) and (28) are thus reduced to two algebraic equations with E_0 and ω_0^2 unknown at the advance time level on one side of the equations and the rest of all known variables from the previous time level on other sides. The iteration procedure of the solution starts by guessing the initial values of E_0 and ω_0 in such a way that they satisfy the boundary conditions (29) and (30), and new values of E_0 and ω_0 are then obtained. These new values are then used again as initial values for the next iteration over time. At each time step (26) is integrated to yield the velocity profile U_0. These computational cycles are repeated until a steady state is judged to have been achieved in which changes in U_0, E_0 and ω_0 are less than 0.5% over the last thousand cycles. For most cases, we found that $N = 41$ gives satisfactory results, and about 3000–5000 cycles are needed to reach a steady state.

The numerical results of the calculated velocity profiles for several values of surface-roughness parameter $u_* y_0/\nu$ are shown in figure 1, which is almost identical with the results of Saffman & Wilcox using a different numerical method. The profile shows how the mean velocity U_0 behaves inside the viscous-sublayer region and how it merges into the logarithmatic velocity distribution outside the sublayer. The velocity profile for $u_* y_0/\nu = 0.12$ is in good agreement with the experimental data of Nikuradse and Reichart (see Schlichting 1961) for smooth wall. The results of calculations of turbulent flow over the undisturbed water surface (which will be called the reference flow) will be used to calculate the linear perturbed flow.

The linearized perturbation equations (31)–(35) and the corresponding boundary conditions (36) and (37) are solved numerically using a finite-difference method. The transformation (38) is again used and, also, the interval of the integration in z is divided into N equal parts. To solve the two-point boundary-value problem by the method of finite differences, all derivatives appearing in the equations are replaced by central-difference approximations for greater accuracy, except that a forward second-order scheme is used for the pressure derivative near the surface boundary.

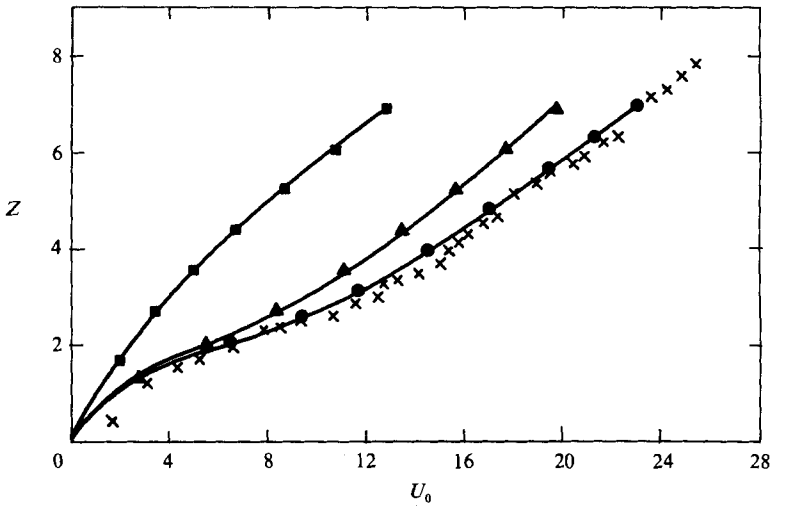

FIGURE 1. Velocity profile U_0 (scaled by u_*) over still water: ●, smooth flow ($u_* y_0/\nu = 0.12$); ▲, transitional flow ($u_* y_0/\nu = 0.28$); ■, rough flow ($u_* y_0/\nu = 8$); ×, experimental data of Nikaradse and Reichardt for smooth flow.

After algebraic manipulations, the linear ordinary differential equations (31)–(35) are reduced to a system of algebraic equations of the form (for details see Al-Zanaidi 1982)

$$\boldsymbol{A}\boldsymbol{Y} = \boldsymbol{R} \tag{39}$$

where $\boldsymbol{A}$, $\boldsymbol{Y}$ and $\boldsymbol{R}$ are the complex coefficient matrix, the unknown complex vector, and the known complex vector respectively. The linear system $\boldsymbol{A}\boldsymbol{Y} = \boldsymbol{R}$ has been solved using the subroutine LEQTIC, which uses the triangular decomposition (i.e. $\boldsymbol{A} = \boldsymbol{A}_\ell \boldsymbol{A}_u$, where $\boldsymbol{A}_\ell$, $\boldsymbol{A}_u$ are lower and upper triangular matrices respectively) of a rowwise permutation of the matrix $\boldsymbol{A}$.

The accuracy attainable with a finite-difference method clearly depends upon the order of the finite-difference approximation and upon the fineness of the mesh. In the present numerical model a second-order finite-difference approximation is used for every derivative appearing in the system of ordinary differential equations to obtain higher accuracy. As to the number of mesh points, since the results of a numerical experiment show that the difference in the values of the energy inputs to the wave for $N = 40$ and $N = 50$ is of the order of 1 %, it was decided to use $N = 40$ for all computations, for which the rank of the matrix is 200.

4. Numerical results and comparisons with experiments and other calculations

4.1. *Introduction*

Although it is well known that both surface-pressure and shear-stress variation along the waves influence the rate of energy transfer between the air flow and the waves, the contribution due to shear-stress variation has been found in our calculation to account for less than 1 % of the total (Al-Zanaidi 1982) and will thus be neglected.

The wave-perturbation pressure p is proportional to the wave slope ak and may be written in one of the following forms:

$$p = ak\left(\frac{\alpha}{\sigma}+\mathrm{i}\frac{\beta}{\sigma}\right)\rho_{\mathrm{w}}c^2\exp(\mathrm{i}kx) \tag{40a}$$

or

$$p = ak(\delta_{\mathrm{r}}+\mathrm{i}\delta_{\mathrm{i}})\,\rho(U_\lambda-c)^2\exp(\mathrm{i}kx), \tag{40b}$$

where ρ and ρ_{w} are the densities of air and of water. The various growth rates ζ, δ_{i} and β are related by

$$\zeta = \frac{\beta}{\sigma} = \delta_{\mathrm{i}}\frac{\rho}{\rho_{\mathrm{w}}}\left(\frac{U_\lambda}{c}-1\right)^2, \tag{41}$$

and U_λ is the wind speed at the height of one wavelength, which is calculated from (43) below.

As already mentioned in §3.1, there are three independent parameters that define a flow situation. These may be the set of dimensional variables consisting of the wavelength $\lambda = 2\pi/k$, the roughness length y_0 and the friction velocity u_*. Alternatively they may be the set of non-dimensional parameters

$$\frac{U_\lambda}{c}, \quad \frac{c}{(g\nu)^{\frac{1}{3}}}, \quad \frac{u_* y_0}{\nu}, \tag{42}$$

where the first parameter represents the strength of the wind velocity, the second is related to the wavelength, and the third is the non-dimensional surface roughness length (the roughness Reynolds number). For all the calculations we used $\nu = 0.15$ cm^2/s and $g = 981$ cm/s^2.

4.2. *Vertical structure of the wind field*

The turbulent closure model used here automatically produces a logarithmic mean wind structure away from the wave surface, i.e.

$$U = \frac{u_*}{\kappa}\ln\frac{y}{y_0} \quad (y \gg y_0). \tag{43}$$

In figure 2(*a*) is plotted the in-phase component δ_{r} in (42*b*) versus the normal distance η measured from the wave surface, i.e.

$$\eta = y - a\,\mathrm{e}^{-ky}\cos kx. \tag{44}$$

Included are also the results of the potential-flow theory and the field measurements of Snyder *et al.* (1981). The present calculations show that the perturbation pressure decays exponentially away from the wave surface. The calculated rate of decay is also found to be in close agreement with the measurements of Snyder *et al.*, in which the flow was transitional. It is noted that potential-flow theory tends to overestimate the rate of decay.

Calculations for the decay of the out-of-phase component δ_{i} away from the wave surface give similar results. On the other hand, figure 2(*b*) shows that the phase shift angle $\phi = \tan^{-1}(-\beta/\alpha) = \tan^{-1}(-\delta_{\mathrm{i}}/\delta_{\mathrm{r}})$ is almost unchanged as the height increases. All these are in agreement with an important finding of Snyder *et al.* that the wave perturbation pressure decays exponentially in the normal distance from the wave surface without change of phase.

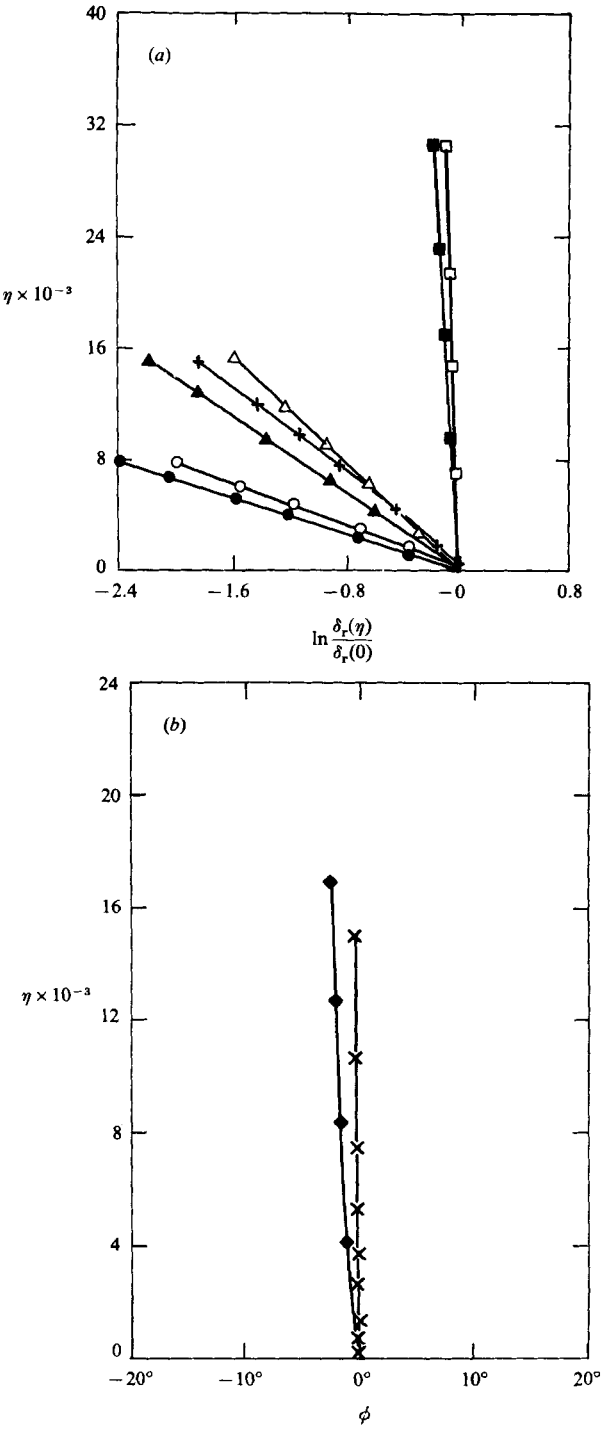

FIGURE 2. (*a*) Vertical structure of the in-phase component of pressure field. Case (i): ○, smooth flow ($U_\lambda/c = 3.0$, $c/(g\nu)^{\frac{1}{3}} = 31.4$, $u_* y_0/\nu = 0.12$); ●, potential theory. Case (ii): +, transitional flow ($U_\lambda/c = 3.0$, $c/(g\nu)^{\frac{1}{3}} = 40.2$, $u_* y_0/\nu = 0.25$); ▲, potential theory; △, Snyder *et al.* (1981). Case (iii): □, rough flow ($U_\lambda/c = 3.0$, $c/(g\nu)^{\frac{1}{3}} = 127.5$, $u_* y_0/\nu = 8$); ■, potential theory. (*b*) Vertical structure of phase shift ϕ from wave trough for the case $U_\lambda/c = 3.0$, $c/(g\nu)^{\frac{1}{3}} = 40.2$, $u_* y_0/\nu = 0.25$: ×, present; ◆, Snyder *et al.* (1981).

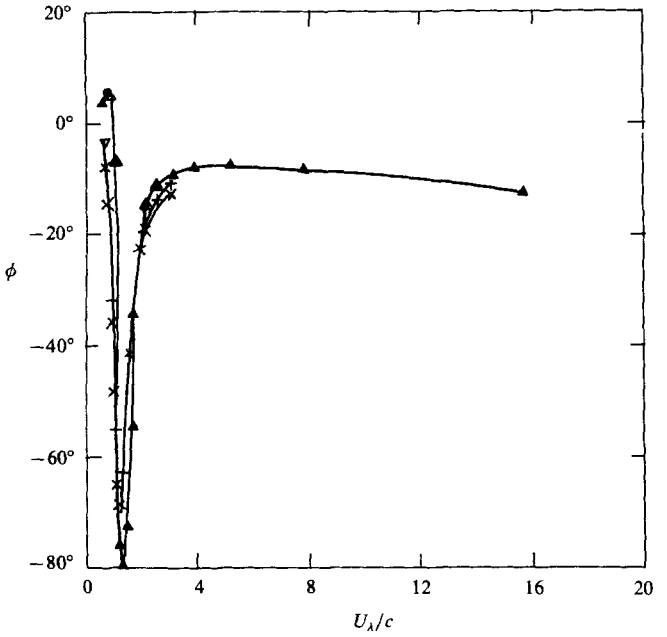

FIGURE 3. The phase shift of the surface pressure from the wave trough for Miles' (1959) parameter $\Omega = \kappa^2 g y_0/u_*^2 = 6.18 \times 10^{-4}$. ▲, transitional flow ($u_* y_0/\nu = 0.223$); +, runs 15–20; ×, runs 14–20 of the field measurements of Snyder *et al.* (1981).

4.3. *The phase-shift angle ϕ of surface pressure*

Observations of the wind-wave generation process at sea (Dobson 1971; Elliott 1972; Snyder 1974; Snyder *et al.* 1981) all have one aim in common, namely to determine the phase shift from the wave trough in the pressure signal. In order to compare the results of Snyder *et al.* with our model, the parameters for their measurement have been established from their table II. The average wind speed at 5 m and the average friction velocity for runs 15–20 are 643.7 cm/s and 20.4 cm/s respectively. The magnitude of the surface-roughness parameter ($u_* y_0/\nu = 0.223$) shows that the flow is transitional in the field. The computations of the phase shift of the pressure signal as a function of U_λ/c are shown in figure 3 along with runs 15–20 and runs 14–20 of Snyder *et al.* The present calculations are in good agreement with their results. Their maximum phase shift of the surface pressure is 80°, and it occurs at $U_\lambda/c \approx 1.3$. Our calculated maximum shift is 10% larger and the shape of the curve is sharper than that of Snyder *et al.* The pressure phase is almost constant ($\approx 8°$) for U_λ/c between 3 and 8, which corresponds to short waves. The position of the phase peak lies in the range $1.0 < U_\lambda/c < 2.0$; that is, when the waves travel with a phase velocity comparable to the wind velocity. There is also another peak at $U_\lambda/c \approx 1.0$ where the pressure phase shift changes sign as the wave moves with phase velocity comparable to or faster than the wind speed. This implies energy transfer from wave to the mean airflow, as expected.

However, present calculations of the fractional rate of energy input per radian from wind for transitional flow are about two-thirds as large as the lowest of the curves of Snyder *et al.*, particularly near the spectral peak for which $U_\lambda/c \approx 1.6$ (Al-Zanaidi 1982). The difference of the pressure amplitude between the present calculation and

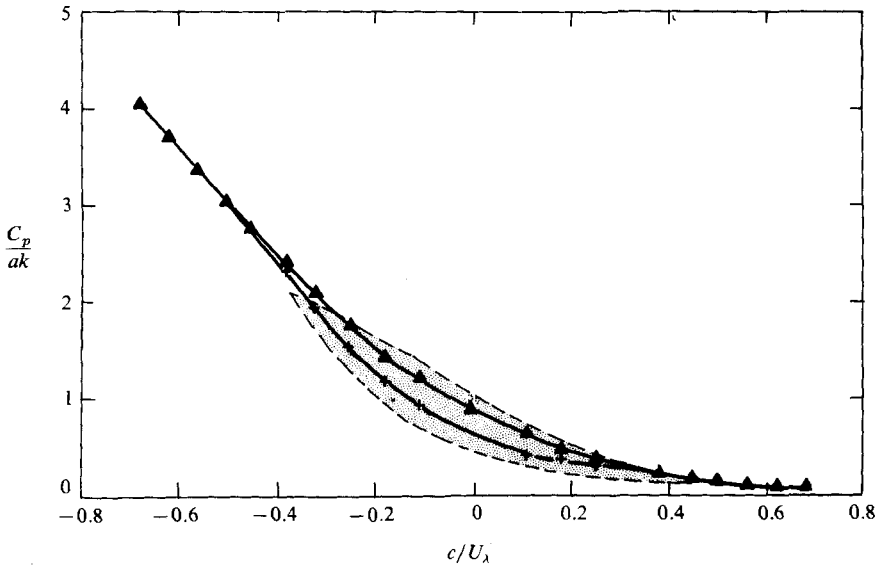

FIGURE 4. Wave perturbation-pressure coefficient. The various measurements of Kendall (1970) fall within the shaded area. Present calculations for Miles' parameter $\Omega = \kappa^2 g y_0/u_*^2 = 3 \times 10^{-3}$ are: +, smooth flow ($u_* y_0/\nu = 0.15$); ▲, rough flow ($u_* y_0/\nu = 8.0$).

the field measurement of Snyder *et al.* may be due to the nature of the waves in the ocean, in that they are moving in a group, consisting of both larger and smaller waves, whereas in our mathematical model they are Stokes waves of infinite train.

4.4. *The pressure coefficient*

As shown in figure 4, comparisons with the data of Kendall (1970) indicate that the present model predicts the magnitude of the wave-perturbation pressure coefficient

$$C_p = 2ak\left(1-\frac{c}{U_\lambda}\right)^2 (\delta_r^2+\delta_i^2)^{\frac{1}{2}} \tag{46}$$

with reasonable accuracy. The effects of surface roughness is clearly demonstrated, especially for small absolute values of c/U_λ, where the pressure coefficient C_p due to rough flow ($u_* y_0/\nu = 8$) is large compared with its values for smooth flow ($u_* y_0/\nu = 0.15$). This shows the sensitivity of the surface-roughness conditions and the indirect effect of viscous sublayer (in the case of smooth flow) on the pressure coefficient.

4.5. *Comparisons with other calculations*

In comparing our results with Conte & Miles' (1959) calculations, we shall consider smooth, transitional and rough flows. Numerical results in terms of Miles' wave-growth parameter β_M (equal to β used in Miles) are plotted in figure 5 for $\Omega = \kappa^2 g y_0/u_*^2 = 3 \times 10^{-3}$ along with Conte & Miles' calculations. The growth parameter β_M is related to δ_i by the following relation:

$$\beta_M = \kappa^2 (U_\lambda - c)^2 \delta_i. \tag{47}$$

In the figure, the present β_M and Conte & Miles' β are seen to be close for transitional and rough flow conditions in the range $c/u_* = 8$–12. This supports Phillips' (1977,

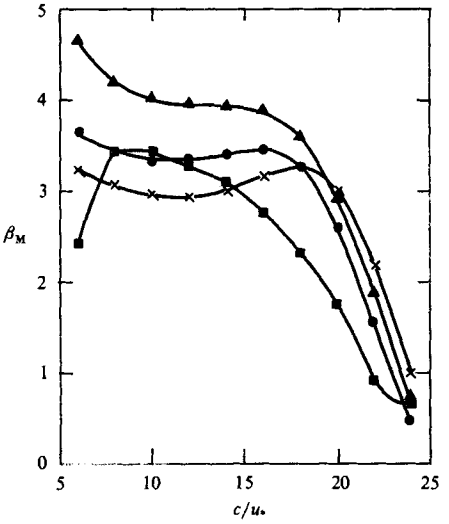

FIGURE 5. The out-of-phase component β_M of surface pressure for $\Omega = \kappa^2 g y_0/u_*^2 = 3\times10^{-3}$: ▲, smooth flow ($u_* y_0/\nu = 0.15$); ●, transitional flow ($u_* y_0/\nu = 0.25$); ×, rough flow ($u_* y_0/\nu = 8$); ■, Conte & Miles (1959).

§4.3) argument that Miles' formula is expected to become important in a narrow range of $c/u_* \approx 10$. For $c/u_* < 8$ and $c/u_* > 14$, however, the calculated results are larger compared with Conte & Miles' values. The following explanations for the difference are given. First, Miles' critical layer (where the wave and wind speed are matched) is moving closer to the wave surface as c/u_* decreases; that is, it lies closer to or within the viscous-sublayer region. In this region, the viscous effect is expected to dominate the flow. But Miles' model is inviscid, so his prediction of β_M may be inaccurate for small values of c/u_*. Secondly, for large c/u_*, the energy input to the wave in Miles' model depends on the existence and the height of the critical layer. The magnitude of Miles' β_M for large c/u_* may be underestimated owing to the large height of the critical layer. Thirdly, the interaction of turbulent air flow with waves is included in the present model but neglected in Miles'.

On the other hand, the calculated in-phase components of surface pressure are in good agreement with Conte & Miles' calculations (see Al-Zanaidi 1982).

Comparisons of the present calculations with that of Townsend (1972), and Gent & Taylor (1976) for waves travelling in the wind direction show order-of-magnitude agreement for the rate of energy input to the waves (Al-Zanaidi 1982), with the present calculations predicting a rate that is consistently up to 50 % higher. It should be noted that their models assumed the flow to be hydraulically rough to avoid the difficulties arising from the viscous sublayer, while field data of Snyder *et al.* (1981) indicate that typical airflow over ocean waves is transitional.

Under adverse wind conditions, on the other hand, the airflow over waves is more likely to be hydraulically rough. Gent (1977) has calculated the rate of attenuation of waves travelling against wind, assuming a rough flow condition. His results are compared with ours (for the case of rough flow) in table 1 for various values of the parameter

$$R = -\ln(ky_0) \tag{48}$$

and c/u_*. Good agreements of the two calculations are seen for both the pressure

		Gent (1977)			Present model		
R	$\frac{c}{u_*}$	$-\mathrm{Re}\left(\frac{P_1}{C^2}\right)$	$-\mathrm{Im}\left(\frac{P_1}{C^2}\right)$	ϕ	$-\mathrm{Re}\left(\frac{P_1}{C^2}\right)$	$-\mathrm{Im}\left(\frac{P_1}{C^2}\right)$	ϕ
6.0	−3.0	24.44	2.890	6.74°	36.47	3.500	5.48°
7.0	−5.0	15.00	1.200	4.57°	16.14	1.390	4.92°
8.0	−8.0	9.53	0.563	3.38°	9.60	0.585	3.49°
9.0	−14.0	5.64	0.224	2.28°	5.37	0.220	2.34°
10.0	−22.0	3.95	0.112	1.62°	4.23	0.107	1.45°

TABLE 1. Comparison of surface-pressure components and phase shift for various values of R and c/u_*. The waves are travelling against the wind.

components and the phase-shift angle. Both calculations also show a rate of attenuation that is of the same order of magnitude as in the generation case. The attentuation rate is typically 10^2–10^3 times larger than the viscous damping.

4.6. *Typical results for a given wavetrain*

In figure 6(*a*), the fractional rate of energy transfer per radian is plotted as a function of the ratio (U_λ/c) of wind speed at one wavelength height over the wave phase velocity for a wavetrain with wavelength $\lambda = 10$ m and various flow conditions. In the figure the positive values of U_λ/c correspond to the wavetrain travelling with the wind, and the negative values of $U_\lambda/c < 0$ correspond to the wavetrain travelling against the wind. It is clear that the predicted rate of energy transfer is from the wind to the wave when the wave is travelling with the wind, except when the wave is travelling at a velocity slightly faster than the wind ($1 < U_\lambda/c \leqslant 1.1$); in the latter case the energy transfer is predicted to be from the wave to the wind. On the other hand, the energy transfer is predicted to be from the wave to the wind when the wave is travelling against the wind, as would be expected intuitively. In figure 6(*a*), the rate of attenuation of a wave opposing the wind is seen to be comparable to the rate of energy input to the wave moving with the wind for all surface-roughness conditions. Moreover, both the rate of energy input (generation) and the rate of attenuation are increased as the surface roughness increases, especially for large absolute values of U_λ/c.

For wavetrains of different wavelengths the rates of energy transfer to and from the waves show similar behaviour to that of figure 6(*a*). It is observed that the curves of figure 6(*a*) have approximately a parabolic form. Indeed, when they are plotted as a function of $(U_\lambda/c-1)^2$, we obtain approximate linear relations (figure 6*b*) between the energy transfer $(\rho_w/\rho)\,\zeta$ and $(U_\lambda/c-1)^2$. These will be discussed further in §5.

The corresponding surface-pressure phase shift ϕ from the wave trough for conditions of figure 6 is shown in figure 7 as a function of U_λ/c. As shown in figure 7, the phase shift is positive and small for a wave travelling against the wind, but is negative and can be large for a wave travelling with the wind. Also, the phase shift has an absolute maximum value of about 80° which occurs within the range $1 \leqslant U_\lambda/c \leqslant 2$. Both present prediction of the surface pressure phase shift and Snyder's (1974) observation show that the phase shift changes sign when the waves are travelling at speeds comparable to those of the wind. Furthermore, the effect of the surface-roughness conditions on the phase shift for waves travelling with the wind is larger compared with that for waves travelling against the wind.

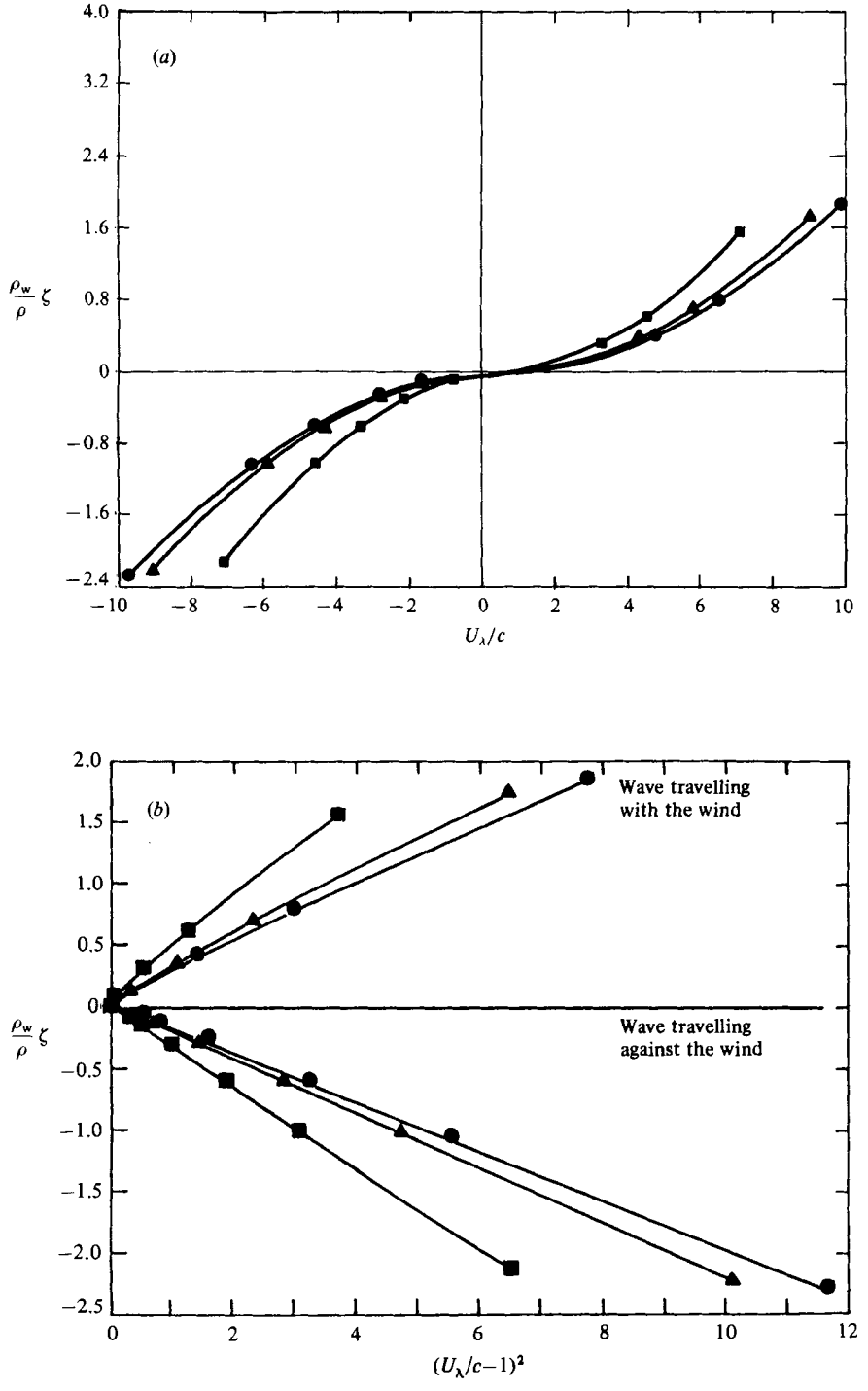

FIGURE 6. (*a*) Fractional rate of energy transfer per radian $(\rho_w/\rho)\zeta$ versus U_λ/c for a 10 m wave. (*b*) $(\rho_w/\rho)\zeta$ versus $(U_\lambda/c-1)^2$. ●, smooth flow $(u_* y_0/\nu = 0.12)$; ▲, transitional flow $(u_* y_0/\nu = 0.25)$; ■, rough flow $(u_* y_0/\nu = 8.0)$.

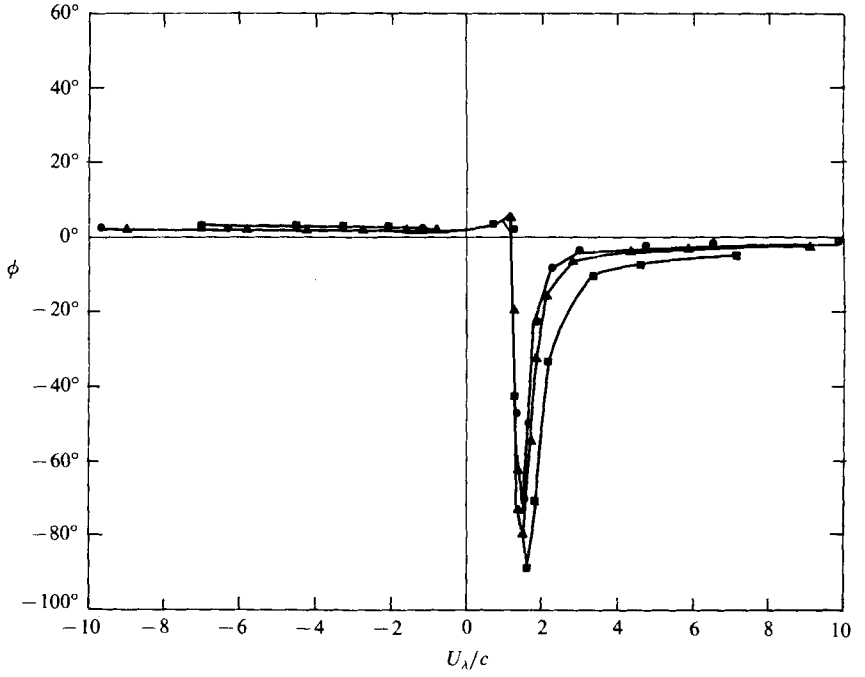

FIGURE 7. The phase shift of the surface pressure from the wave trough for a 10 m wave ($c/(g\nu)^{\frac{1}{3}} = 74.8$). For legend see figure 6.

5. Concluding remarks

In the present model of turbulent airflow over a train of Stokes waves of small amplitude, there are three independent parameters defining a flow situation. Systematic computations for the combinations of the three parameters over wide ranges were done to determine how the rate of energy transfer between wind and wave varies with each of the parameters. From these computations it emerged, as noted in §4.6 (figure 6*b*), that the fractional rate of energy transfer per radian ζ is approximately proportional to $(U_\lambda/c-1)^2$ for a given wavetrain. This implies that δ_i in (40*b*) depends only on two independent parameters: the wavelength λ (or equivalently $c/(g\nu)^{\frac{1}{3}}$) and the roughness parameter $u_* y_0/\nu$. This out-of-phase coefficient δ_i is plotted as a function of wavelength λ in figure 8 for the case of favourable wind and in figure 9 for the case of adverse wind. It is seen that δ_i, and hence the rate of energy transfer, depends critically on the flow being hydraulically transitional or rough. On the other hand, it varies rather gently with wavelength.

For the generation case, i.e. when $U_\lambda/c > 1$, δ_i takes approximately the value of 0.04 if the flow is transitional or smooth. For rough flow, on the other hand, δ_i increases with wavelength from 0.05 to 0.07. Thus we have the following approximate formula for the fractional rate of energy input by wind per radian:

$$\zeta = \frac{\beta}{\sigma} = \delta_i \frac{\rho}{\rho_w}\left(\frac{U_\lambda}{c}-1\right)^2, \tag{49a}$$

with

$$\delta_i = \begin{cases} 0.04 & \text{(for smooth or transitional flow)}, \\ 0.06 \pm 0.01 & \text{(for rough flow)}. \end{cases} \tag{49b}$$

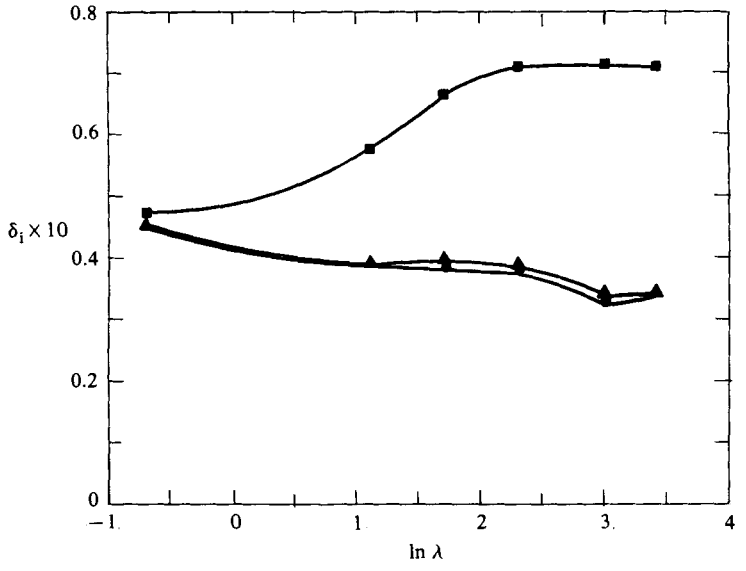

FIGURE 8. The out-of-phase coefficient δ_i for waves travelling with the wind $U_\lambda/c > 1$. For legend see figure 6.

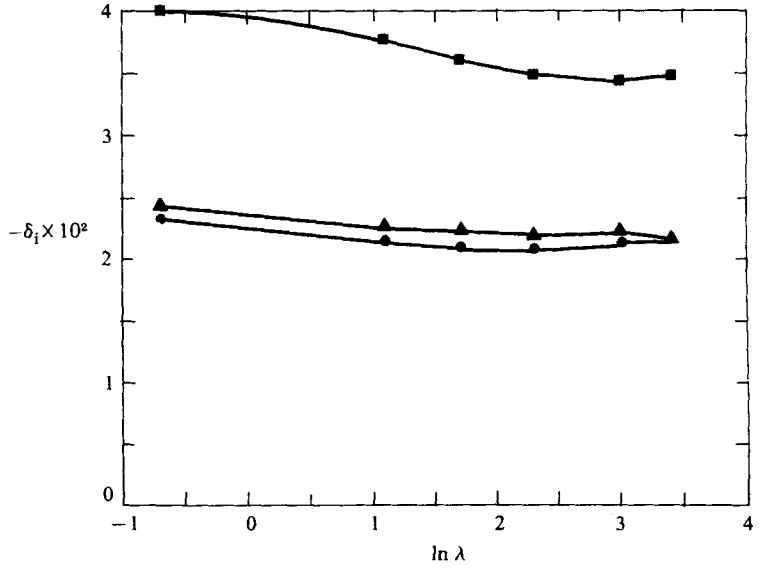

FIGURE 9. The out-of-phase coefficient δ_i for waves travelling against wind $U_\lambda/c < 0$. For legend see figure 6.

Equation (49*a*) with values of δ_i given by (49*b*) is plotted in figure 10 in comparison with most existing experimental data as compiled by Plant (1982). In this figure we use $\rho/\rho_w = 0.0125$, $U_\lambda = 25u_*$ and $\delta_i = 0.06$ for rough flow. As noted in §1, ocean wind waves (e.g. Snyder *et al.* 1981) correspond to transitional flow, and should be compared with $\delta_i = 0.04$. The agreement of our calculations with experimental data is seen to be good for a wide range of u_*/c from ocean waves to laboratory waves.

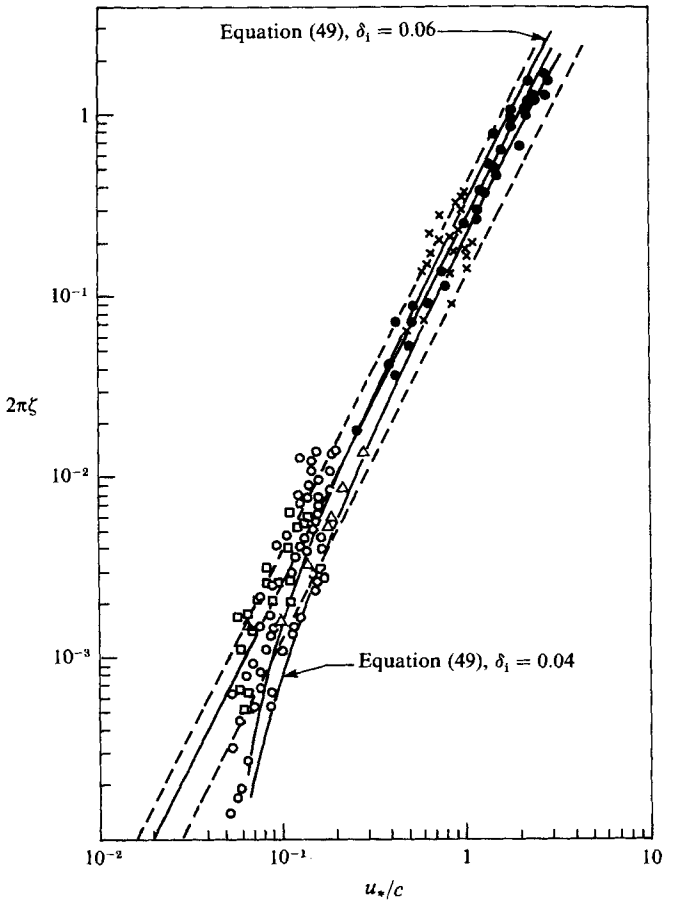

FIGURE 10. Fractional rate of energy input from wind to wave per wave period versus friction velocity per unit phase velocity. Straight solid and dashed lines, Plant (1982); △, Shemdin & Hsu (1967); ●, Larson & Wright (1975); ×, Wu *et al.* (1977, 1979); ○, Snyder *et al.* (1981), fixed sensors; □, Snyder *et al.* (1981), wave-following sensor; solid curves, equation (49).

For large U_λ/c, (49) reduce to

$$\zeta = \frac{\beta}{\sigma} = \begin{cases} 0.031\left(\dfrac{u_*}{c}\right)^2 & \text{(for smooth or transitional flow)}, \quad (50a) \\ 0.047\left(\dfrac{u_*}{c}\right)^2 & \text{(for rough flow)}, \quad (50b) \end{cases}$$

which is in excellent agreement with Plant's empirical formula (1). The latter, however, does not distinguish transitional or smooth flow from rough flow.

Formula (49a) with $\delta_i = 0.04$ is also in excellent agreement with Stewart's (1974) formula

$$\frac{\beta}{\sigma} = 0.04\,\frac{\rho}{\rho_w}\left[\left(\frac{U_5}{c}\right)^2 - \frac{U_5}{c}\right], \quad (51)$$

especially if the wind velocity at 5 m height, U_5, is large compared with the phase velocity c.

More recently, wave-tank experiments by Mitsuyasu & Honda (1982) yielded the result

$$\frac{\beta}{\sigma} = \frac{0.34}{2\pi}\left(\frac{u_*}{c}\right)^2 = 0.054\left(\frac{u_*}{c}\right)^2. \tag{52}$$

Since the flow in their experiment was rough, and the values of U_λ/c were large, their results should be compared with our (50*b*). The agreement is again seen to be good.

In the case of wind blowing against waves, we have, from figure 9,

$$\delta_i = \begin{cases} -0.024 & \text{(for smooth or transitional flow),} \\ -0.040 & \text{(for rough flow).} \end{cases} \tag{53}$$

It should be pointed out that, in the case of wind blowing against waves, the flow is most probably rough, and the value of $\delta_i = -0.04$ shold be used accordingly. Preliminary data from the experiments conducted by Dr M. A. Donelan at the Canada Centre for Inland Waters wind-wave flume using a wave follower indicates the constancy of δ_i for the cases of wind blowing against waves. Further detailed comparisons between present calculation and experiments will be made in the near future.

In conclusion, our systematic numerical calculations have been shown to be in good agreement with most existing experimental data covering a wide range of conditions for waves on the ocean and those in wave tanks.

If, as is likely, the flow is transitional under favourable wind conditions and rough under adverse wind conditions, then the growth rate for $U_\lambda/c > 1$ and the attenuation rate for $U_\lambda/c < 0$ are given simply by (49*a*) with

$$|\delta_i| = 0.04. \tag{54}$$

We are indebted to Dr M. A. Donelan for many valuable discussions during the course of research. Thanks are also due to Dr P. A. Taylor for his comments on the work. This work was supported by the Natural Sciences and Engineering Research Council of Canada.

REFERENCES

Al-Zanaidi, M. A. 1983 Water wave generation and attenuation by wind – a numerical study. Ph.D. thesis, University of Waterloo.

Conte, S. & Miles, J. W. 1959 On the numerical integration of the Orr–Sommerfeld equation. *J. Soc. Indust. Appl. Maths* **7**, 361–366.

Davis, R. E. 1969 On the high Reynolds number flow over a wavy boundary. *J. Fluid Mech.* **36**, 337–346.

Davis, R. E. 1970 On the turbulent flow over a wavy boundary. *J. Fluid Mech.* **42**, 721–731.

Davis, R. E. 1972 On prediction of the turbulent over a wavy boundary. *J. Fluid Mech.* **52**, 287–306.

Davis, R. E. 1974 Perturbed turbulent flow, eddy viscosity and generation of turbulent stresses. *J. Fluid Mech.* **63**, 673–693.

Dobson, F. W. 1971 Measurements of atmospheric pressure on wind-generated sea waves. *J. Fluid Mech.* **48**, 91–127.

Elliott, J. A. 1972 Microscale pressure fluctuations near waves being generated by wind. *J. Fluid Mech.* **54**, 427–448.

Gent, P. R. 1977 A numerical study of air flow above water waves. Part 2. *J. Fluid Mech.* **82**, 349–369.

GENT, P. R. & TAYLOR, P. A. 1976 A numerical model of air flow above water waves. *J. Fluid Mech.* **77**, 105–128.

HSU, C. T., WU, H. Y., HSU, E. Y. & STREET, R. L. 1982 Momentum and energy transfer in wind generation of waves. *J. Phys. Oceanogr.* **12**, 929–951.

KAWAI, S. 1979 Generation of initial wavelets by instability of a coupled shear flow and their evolution to wind waves. *J. Fluid Mech.* **93**, 661–703.

KENDALL, J. M. 1970 The turbulent boundary layer over a wall with progressive surface waves. *J. Fluid Mech.* **41**, 259–281.

KOLMOGOROV, A. N. 1942 Equations of turbulent motion of an incompressible fluid. *Izv. Akad. Nauk SSSR Ser. Fiz.*, VI, no. 1–2, pp. 56–58.

LARSON, T. R. & WRIGHT, J. W. 1975 Wind-generated gravity–capillary waves: laboratory measurements of temporal growth rates using microwave backscatter. *J. Fluid Mech.* **70**, 417–436.

LAUNDER, B. E. & SPALDING, D. B. 1972 *Lectures in Mathematical Models of Turbulence.* Academic.

MARVIN, J. G. 1983 Turbulent modeling for computational aerodynamics. *AIAA J.* **21**, 941–955.

MILES, J. W. 1957 On the generation of surface waves by shear flows. *J. Fluid Mech.* **3**, 185–204.

MILES, J. W. 1959 On the generation of surface waves by shear flows. Part 2. *J. Fluid Mech.* **6**, 568–582.

MILES, J. W. 1967 On the generation of surface waves by shear flows. Part 5. *J. Fluid Mech.* **30**, 163–175.

MITSUYASU, H. & HONDA, T. 1982 Wind-induced growth of water waves. *J. Fluid Mech.* **123**, 425–442.

PHILLIPS, O. M. 1957 On the generation of waves by turbulent wind. *J. Fluid Mech.* **2**, 417–445.

PHILLIPS, O. M. 1977 *Dynamics of the Upper Ocean*, 2nd edn. Cambridge University Press.

PLANT, W. J. 1982 A relationship between wind stress and wave slope. *J. Geophys. Res.* **87**, 1961–1967.

RILEY, D. S., DONELAN, M. A. & HUI, W. H. 1982 An extended Miles theory for wave generation by wind. *Boundary-Layer Met.* **22**, 209–225.

SAFFMAN, P. G. 1970 A model for inhomogeneous turbulent flow. *Proc. R. Soc. Lond.* A **317**, 417–433.

SAFFMAN, P. G. & WILCOX, D. C. 1974 Turbulence-model predictions for turbulent boundary layers. *AIAA J.* **12**, 541–546.

SHEMDIN, O. H. & HSU, E. Y. 1967 Direct measurement of aerodynamic pressure above a simple progressive gravity wave. *J. Fluid Mech.* **30**, 403–416.

SNYDER, R. L. 1974 A field study of wave-induced pressure fluctuations above surface gravity waves. *J. Mar. Res.* **32**, 497–531.

SNYDER, R. L., DOBSON, F. W., ELLIOTT, J. A. & LONG, R. B. 1981 Array measurements of atmospheric pressure fluctuations above surface gravity waves. *J. Fluid Mech.* **102**, 1–59.

STEWART, R. W. 1970 Laboratory studies of the velocity field over deep-water waves. *J. Fluid Mech.* **42**, 733–754.

STEWART, R. W. 1974 The air–sea momentum exchange. *Bouncary-Layer Met.* **6**, 151–167.

TOWNSEND, A. A. 1972 Flow in a deep turbulent boundary layer over a surface distorted by water waves. *J. Fluid Mech.* **55**, 719–735.

WU, H. Y., HSU, E. Y. & STREET, R. L. 1977 The energy transfer due to air-input, non-linear wave–wave interaction and white cap dissipation associated with wind-generated waves. *Stanford Univ. Tech. Rep.* 207, pp. 1–158.

WU, H. Y., HSU, E. Y. & STREET, R. L. 1979 Experimental study of nonlinear wave–wave interaction and white-cap dissipation of wind-generated waves. *Dyn. Atmos. Oceans* **3**, 55–78.